Physics Letters A 384 (2020) 126707

Contents lists available at ScienceDirect

Physics Letters A

www.elsevier.com/locate/pla

Polarity and bioelectrical patterning in a linear chain of non-excitable cells

Javier Cervera *, José A. Manzanares, Salvador Mafe

Dept. de Termodinàmica, Facultat de Física, Universitat de València, E-46100 Burjassot, Spain

ARTICLE INFO

Article history:
Received 15 April 2020
Received in revised form 22 June 2020
Accepted 29 June 2020
Available online 3 July 2020
Communicated by M. Perc

Keywords:
Bioelectrical head-tail polarity
Non-excitable cells chain model
Ion channels and gap junctions
Multicellular memory

ABSTRACT

Polarity in multicellular systems is influenced by bioelectrical signals because electric potentials can act as spatio-temporal patterns for other biochemical processes that eventually emerge as long-lasting biological outcomes. We study the role of the electric potential in establishing *head-tail* polarity for the case of a chain of non-excitable cells. This biophysical model incorporates both *single-cell* (membrane ion channels) and *multicellular* (intercellular gap junctions) characteristics. The results are presented in the form of a bioelectrical phase space that complements traditional biochemical approaches and provides qualitative insights for the case of anterior/posterior polarity in biological model systems. In particular, we show that simple bioelectric circuits can exhibit complex multicellular patterning, suggesting strategies to establish axial polarity in synthetic biology and regeneration.

1. Introduction

Developmental and regeneration models need to address a crucial question: which mechanisms allow cells to determine their relative spatial position and how these mechanisms can eventually result in biological outcomes characterized by both short and long order polarity. Bioelectrical signals and electrochemical gradients are involved in the establishment of axial polarity and patterning in cells and tissues [1–6]. This problem is however traditionally described in terms of heterogeneous spatio-temporal distributions of specific morphogens [7–10]. In the present simulations, we attempt a bioelectrical description that complements earlier well-established studies focused on reaction-diffusion models. This description is relevant to development and can guide experimental procedures to establish target patterns based on electric potentials. In particular, it could be possible to coordinate cell states by acting on downstream morphogenetic cascades using electric potential patterns [2–4] because these patterns dictate the local concentrations of signaling ions and molecules that regulate regional transcription.

The head-tail development in planaria constitutes a relatively simple model system where the axial patterning processes are usually described on the basis of purely biochemical approaches [8–10]. Experimentally, there exists a significant potential difference between the head and the tail that is consistently maintained during development [2,11,12]. This fact strongly suggests that biochemical gradients are coupled to polar bioelectrical patterns that influence the correct distribution of signaling ions and molecules, as is also the case of other biological systems [3,6,12–15]. Thus, the external regulation of biophysical magnitudes such as electric potentials that are defined at the multicellular level can facilitate the control of large-scale outcomes in a complementary way to acting at the single-cell level [3,4,16,17].

We present here a bioelectrical approach to the long and short range polar patterns that emerge in a linear chain of non-excitable cells. This *toy model* can only mimic complex real systems but it includes two basic biological characteristics: the ion channels whose counteracting action establish individual *single-cell* potentials and the *intercellular* gap junctions that provide multicellular connectivity [2,3,11,14,17]. In a closely related work, detailed simulations focused on bioelectrical patterns in planaria have recently been presented [12,18]. However, we concentrate here on the *long and short-range polarity* of a generic one-dimensional multicellular chains in order to clearly show the basic mechanisms that regulate the system outcomes. While the model is purely bioelectrical, it is well established that bioelectrical and biochemical polarities are interrelated in many biological processes [1–4,12,14].

2. Biophysical model

The model of Fig. 1 considers a linear chain of $N = 100$ cells whose individual bioelectrical state is described by the membrane potential $V < 0$ which is defined as the electric potential difference between the cell inside and the external environment. In cell

* Corresponding author.
E-mail address: javier.cervera@uv.es (J. Cervera).

https://doi.org/10.1016/j.physleta.2020.126707
0375-9601/

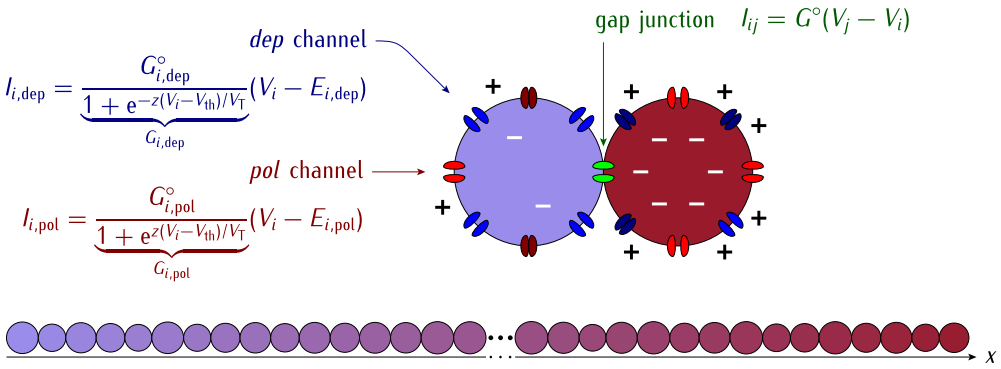

Fig. 1. The bioelectrical polarity is established by the electric potential regionalization of a multicellular linear chain of length $L = Nd$, where N is the number of cells and d is the cell diameter. The potential V_i of cell i ($i = 1, 2, \ldots, N$) changes with time t because of: (1) the single-cell currents $I_{i,\mathrm{pol}}$ and $I_{i,\mathrm{dep}}$ of two generic populations of voltage-gated *pol* and *dep* ion channels [14,19] whose maximum conductances are $G^\circ_{i,\mathrm{k}}$ ($\mathrm{k} = \mathrm{pol},\ \mathrm{dep}$) and (2) the intercellular current $I_{ij} = G^\circ(V_j - V_i)$ through the gap junction of conductance G° established between neighboring cells i and j [14]. In the model, $E_{i,\mathrm{pol}}$ and $E_{i,\mathrm{dep}}$ are the equilibrium potentials, z is the channel gating charge, V_{th} is the threshold potential, and $V_{\mathrm{T}} = RT/F$ is the thermal potential, where R, T, and F are the gas constant, the temperature, and the Faraday constant, respectively [19,20]. In this model, a sufficiently high chain electrical polarity will result in a normal asymmetric (*head-tail*) morphology while a low chain polarity will give an abnormal symmetric morphology (e.g., *head-head* or *tail-tail*) when all cells are in depolarized state [2,11,18].

biophysics, V can be established by the balance of the electric currents of two generic *pol* and *dep* ion channels [19] and the intercellular current flowing through the junction between neighboring cells [14]. The *pol* ($G_{i,\mathrm{pol}}$) and *dep* ($G_{i,\mathrm{dep}}$) channel conductances act to establish the equilibrium potentials $E_{i,\mathrm{pol}}$ and $E_{i,\mathrm{dep}}$ characteristic of the *polarized* and *depolarized* cell states through the currents $I_{i,\mathrm{pol}}$ and $I_{i,\mathrm{dep}}$, respectively [14]. In this approximation, we neglect the small contribution of the ion pump currents to the single-cell potentials and assume that their unique role is to keep constant the ionic concentration differences that maintain the above equilibrium potentials [19].

Following the usual convention, the single-cell currents $I_{i,\mathrm{pol}}$ and $I_{i,\mathrm{dep}}$ of Fig. 1 are positive when the cations flow out of the cell [19,20]. The sign of the intercellular currents I_{ij} depends on the relative potentials of the neighbor cells $j = i \pm 1$ with respect to the central cell i. Because of the high number of cells $N = L/d \gg 1$, we can write these currents as $G^\circ(V_{i-1} - V_i + V_{i+1} - V_i) \approx G^\circ d^2 \partial^2 V/\partial x^2$ in the continuum limit. Thus, the electrical balance equation [4,14] for the individual cells of the multicellular chain can be written as

$$\frac{\partial V}{\partial t} = \underbrace{\left(\frac{G^\circ d^2}{C}\right)}_{D}\frac{\partial^2 V}{\partial x^2} - \underbrace{\left(\frac{G^\circ_{\mathrm{dep}}}{C}\right)}_{1/\tau} \times \left[\frac{G^\circ_{\mathrm{pol}}}{G^\circ_{\mathrm{dep}}}\underbrace{\frac{(V - E_{\mathrm{pol}})}{1+\exp[z(V-V_{\mathrm{th}})/V_{\mathrm{T}}]}}_{I_{\mathrm{pol}}/G^\circ_{\mathrm{pol}}} + \underbrace{\frac{(V - E_{\mathrm{dep}})}{1+\exp[-z(V-V_{\mathrm{th}})/V_{\mathrm{T}}]}}_{I_{\mathrm{dep}}/G^\circ_{\mathrm{dep}}}\right] \tag{1}$$

where C is the cell capacitance, $D = G^\circ d^2/C$ is an effective diffusivity, $\tau = C/G^\circ_{\mathrm{dep}}$ is the characteristic single-cell time, and I_{pol} and I_{dep} the channel currents of Fig. 1. Equation (1) is to be solved for $V(x,t)$ with the boundary and initial conditions

$$\left(\frac{\partial V}{\partial x}\right)_{x=0} = 0 = \left(\frac{\partial V}{\partial x}\right)_{x=L},\ t > 0 \tag{2a}$$

$$V(x, t=0) = V_{\mathrm{pol}},\ 0 \le x \le L \tag{2b}$$

These equations impose no electrical propagation at the chain ends and establish the potential V_{pol} corresponding to the solution of equation (1) for $G^\circ_{\mathrm{pol}}/G^\circ_{\mathrm{dep}} = 0.5$ and $G^\circ = 0$ (isolated cell, $I_{\mathrm{pol}} + I_{\mathrm{pol}} = 0$ in Fig. 1) as the initial cell polarization state throughout the chain, respectively. This potential is close to E_{pol} which depends on the cell inside and outside ionic concentrations [19].

The time-dependent local potential $V(x,t)$ of equation (1) is regulated by the diffusivity D and the characteristic time τ. These bioelectrical parameters define a characteristic velocity $v = D/d = G^\circ d/C$ and a bioelectric coupling length $\lambda = (D\tau)^{1/2} = (G^\circ/G^\circ_{\mathrm{dep}})^{1/2} d$ which are proportional to the intercellular connectivity described by the junction conductance G°. In this biophysical model, the positional information depends on $V(x,t)$ which is regulated at the multicellular level by the length ratio $\lambda/d = (G^\circ/G^\circ_{\mathrm{dep}})^{1/2}$ whose limiting cases are $\lambda/d \le 1$ (isolated independent cells) and $\lambda/d > 1$ (correlated groups of cells).

Note that $V(x,t)$ is also influenced by the single-cell conductance ratio $G^\circ_{\mathrm{pol}}/G^\circ_{\mathrm{dep}}$ that gives the relative contribution of the *pol* and *dep* channels to the cell bioelectrical state. This ratio depends on the prepattern of local transcriptional rates that regulate the *pol* and *dep* channel proteins throughout the chain [14,18]. Mathematical models to describe pattern formation by morphogen gradients have been given and validated for the early embryo of the fruit fly Drosophila as the main experimental example [21]. The resulting morphogen gradients were analyzed on the basis of source-diffusion-degradation equations and transcriptional control by morphogens was discussed within the framework of thermodynamic site occupancy models of gene regulatory regions [21]. Because we focus on bioelectrical rather than on genetic patterns, however, we will introduce the *transcriptional prepattern* through a position-dependent conductance ratio $G^\circ_{\mathrm{pol}}/G^\circ_{\mathrm{dep}}$ that modulates the electric potential obtained from equation (1). This simplifies the coupling between bioelectricity and transcription, which has been previously studied in detail [4,12]. Thus, the voltage-gated channel conductances G_{k} ($\mathrm{k} = \mathrm{pol},\ \mathrm{dep}$) defined as

$$G_{\mathrm{pol}} = \frac{G^\circ_{\mathrm{pol}}}{1+\exp[z(V-V_{\mathrm{th}})/V_{\mathrm{T}}]} \tag{3a}$$

and

$$G_{\mathrm{dep}} = \frac{G^\circ_{\mathrm{dep}}}{1+\exp[-z(V-V_{\mathrm{th}})/V_{\mathrm{T}}]} \tag{3b}$$

can be locally regulated both *transcriptionally* by the assumed dependence of the maximum conductance ratio $G^\circ_{\mathrm{pol}}/G^\circ_{\mathrm{dep}}$ on x and

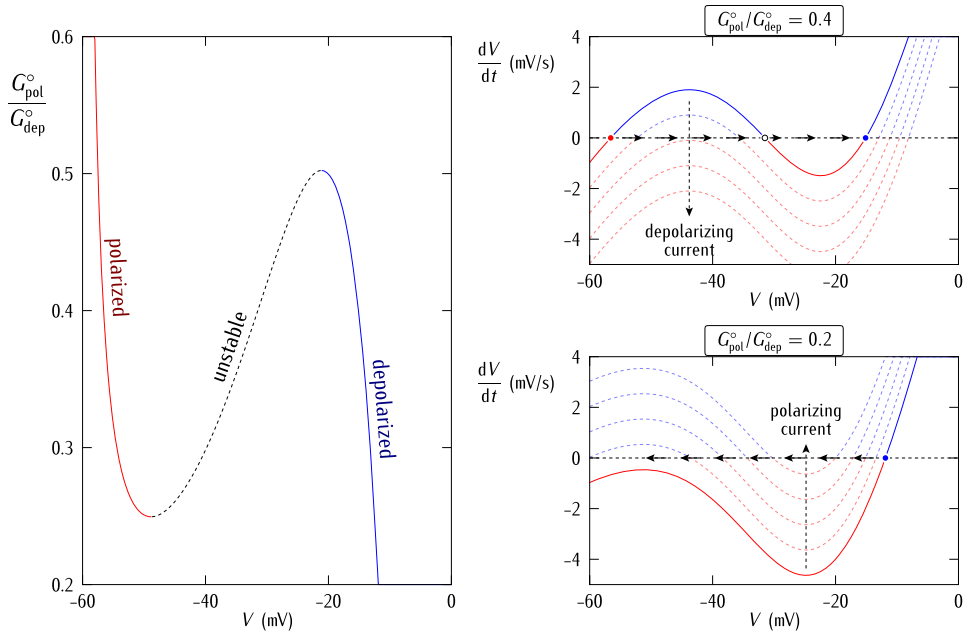

Fig. 2. Bi-stability of the single-cell polarization state [20,22]. The membrane potential V that determines the bioelectrical state of an isolated cell is defined from the zero current condition $I_{pol} + I_{dep} = 0$, where the *pol* and *dep* currents are those of Fig. 1, and is regulated by the conductances G°_{pol} and G°_{dep} and the equilibrium potentials $E_{pol} = -60$ mV and $E_{dep} = -10$ mV (*left*). Note that there is one unstable solution between the two stable solutions in the bi-stability region of the isolated cell. However, these solutions and their corresponding bioelectrical states can be modified in non-isolated cells because V changes with time t when the cations flow inside (*depolarizing current*) and outside (*polarizing current*) the cell to give a non-zero current (right). The effects of these currents are schematically shown for the cases: (1) $G^\circ_{pol}/G^\circ_{dep} = 0.4$ (*right* and *top*, *continuous curve*) where two stable polarized (*red* point) and depolarized (*blue* point) solutions are possible and (2) $G^\circ_{pol}/G^\circ_{dep} = 0.2$ (*right* and *bottom*, *continuous curve*) where only the stable depolarized solution is possible. In both cases, the different currents assumed can shift the initial cell state (*continuous curve*) to other states (*dashed curves*). (For interpretation of the colors in the figure(s), the reader is referred to the web version of this article.)

post-translationally by the potential $V(x,t)$ [14]. This *mixed transcriptional and bioelectric local control* has been described with detail recently [18] and leads to response times ranging from fast electrical relaxations of the order of seconds to slow transcriptional processes that can take hours [22–24]. The rapidly established bioelectrical pattern (seconds to minutes) influences long-term biochemical processes whose times are on the order of hours to days. The above facts make equation (1) different from the cable equation that describes the electrical conduction in excitable cells whose electrical times are of the order of miliseconds [19].

We take here the following typical values [14,19,20] $d = 10$ µm, $z = 3$, and $V_{th} = -V_T = -26$ mV for the system parameters and introduce the conductance $G_{ref} = G^\circ_{dep}$ throughout to scale the single-cell G°_{pol} and intercellular G° conductances to the same reference value. For $G_{ref} = 100$ pS and the cell capacitance $C = 100$ pF, the single-cell electric time is $\tau = C/G_{ref} = 1$ s which is much higher than excitable cell times of the order of 10 ms [19]. As to the characteristic velocity, we have $v = G^\circ d/C = 10$-100 µm/s for junction conductances in the range $G^\circ = 100$-100 pS, where $v = 10$ µm/s corresponds to 1 cell/s. This velocity is related to an intercellular characteristic time $\tau^\circ = d/v = C/G^\circ = 1$ s. Experimentally, these values are reasonable for depolarization waves in multicellular pancreatic islands [25] and depolarization spreads in *Xenopus* froglets [26].

3. Results and discussion

We analyze first the single-cell currents I_{pol} and I_{dep} defined in equation (1). Fig. 2 (*left*) shows that changes in the independent cell potential V are abrupt at the ends of the bi-stability region where three solutions are possible [20,22]. The two stable solutions obtained under the zero current condition in Fig. 2 (*right*) correspond to polarized and depolarized cells with high and low absolute values of V, respectively, while the central point corresponds to the *unstable* solution [20,22]. The changes with time t of the cell potential V in Fig. 2 (*right*) can be interpreted as the dynamics of the bioelectrical memory that evolves from an initial stable state dictated by $G^\circ_{pol}/G^\circ_{dep}$ (continuous curve) in the case of the non-isolated cell. The vertical arrows qualitatively represent the effects of depolarizing (decreasing *dashed* curves) or polarizing (increasing *dashed* curves) constant currents from the neighboring cells to a central cell. The horizontal arrows schematically show the transitions between the stable cell states due to these currents. Multicellular ensembles of gap junction-connected cells can show experimental N-shaped current-voltage curves and bi-stability phenomena similar to that of Fig. 2 [16,25].

Experimentally, it is the bioelectrical polarity regulated by the electrical potential difference between the chain extremes and the multicellular connectivity that modulates the morphologic outcomes [2,11,18]. This fact suggests that externally-induced transitions between different chain polarities can modify these outcomes. In this model, a sufficiently high chain polarity will result in a normal head-tail outcome while a low polarity will give an abnormal symmetrical morphology [2,11,18]. Thus, we will now focus on the *chain bioelectrical patterns* because they are coupled with downstream biochemical processes to give the long-lasting effects that emerge as biological outcomes [2,14,27–29].

We have solved numerically equation (1) for the conditions of equations (2a) and (2b). In the multicellular chain of Fig. 1 (*bottom*), G°_{dep} is taken to be constant and $G^\circ_{pol}(x)$ is changed so that the conductance ratio $G^\circ_{pol}(x)/G^\circ_{dep}$ depends on the local position x. For the sake of concreteness, we assume a prepattern for $G^\circ_{pol}(x)/G^\circ_{dep}$ where the *pol* channel conductance increases linearly from the leftmost cells to the rightmost cells to establish a conductance difference ΔG°_{pol} through the chain (Fig. 3, *top*). At time $t > 0$, the multicellular connectivity is set on and all cells are influenced by their neighbors. The ensemble as a whole relaxes to a steady state after a time of the order of 1 000 s. This time depends

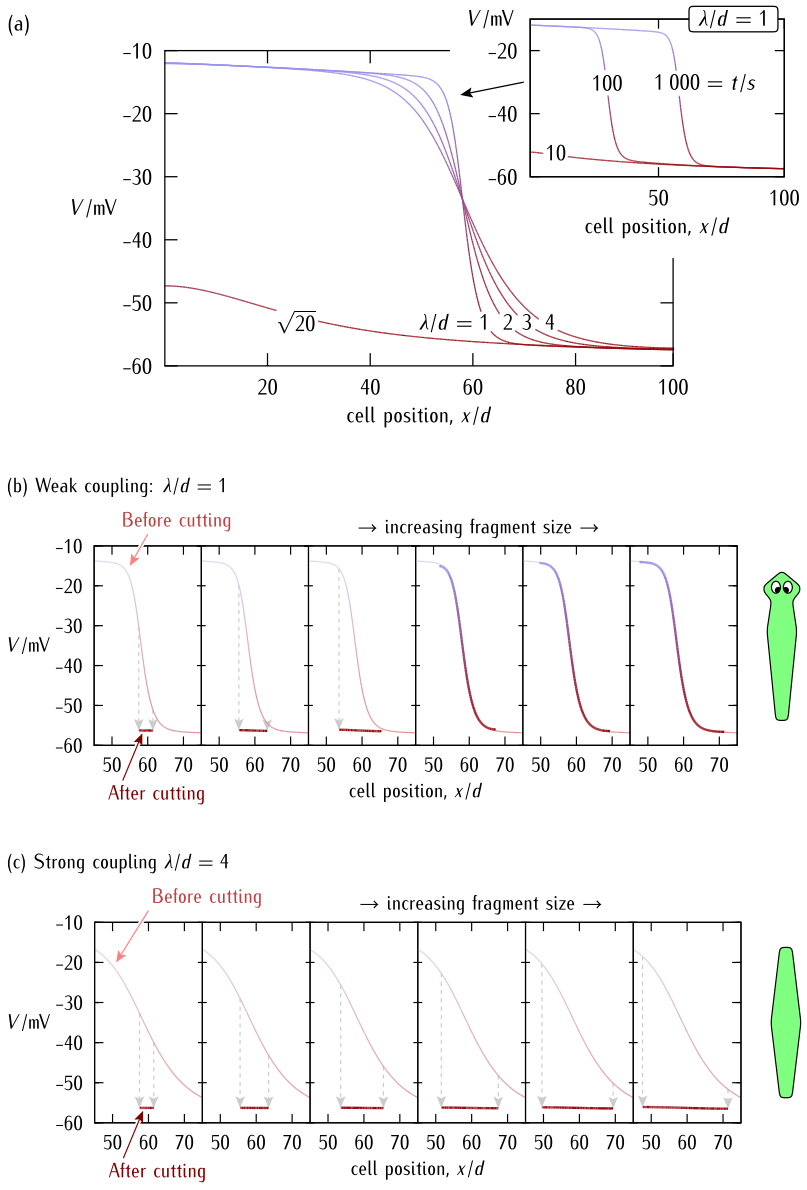

Fig. 3. The steady state electric potential patterns of the multicellular chain obtained from equation (1) for different lengths ratios λ/d, numbers in the curves, (a). The prepattern of *pol* channel conductances is assumed to increase linearly from $G^{\circ}_{pol}/G^{\circ}_{dep} = 0.2$ (cell #1) to $G^{\circ}_{pol}/G^{\circ}_{dep} = 0.5$ (cell #$N = 100$). The initial cell electric potentials $V(x, t = 0) = V_{pol}$ of equation (2b) evolve to the steady state values after times of the order of 1 000 s (*inset*). The inset corresponds to the time evolution of the chain multicellular pattern for the case $G^{\circ}/G^{\circ}_{dep} = 1$. The cutting of a central fragment around the cell #60 in the multicellular system gives subsequent polarity changes (dashed arrows) that depend on the fragment size and intercellular coupling (b and c). Before the cut, the leftmost and rightmost cells of the central fragment have the potentials corresponding to their positions. After the cut, the fragment reaches a new steady state whose polarity depends on the number of cells and the intercellular coupling, characterized by λ/d.

on the single-cell capacitance and channel conductances, the intercellular junction conductance, and the number of cells in the chain; see Fig. 1 and equation (1).

While the multicellular steady state could be either fully depolarized (low absolute value of V) or polarized (high absolute value of V), a central transition region between the depolarized and polarized chain ends is also possible depending on the prepattern of single-cell channel conductances and the intercellular connectivity (Fig. 3, *top*). It is in this case that a steady system polarity can be established from the transcriptional prepattern of ion channel and gap junction proteins [18].

Fig. 3(a) shows that for the single-cell channel asymmetry assumed through the chain, the dominant stable solution corresponds to the polarized chain only for sufficiently high intercellular conductances which correspond to coupling length ratios $\lambda/d \geq \sqrt{20}$ approximately. For low coupling lengths, however, Fig. 3(a) (*inset*) shows that a depolarization pattern can be established through part of the chain only, giving a steady-state potential regionalization where the leftmost cells are depolarized while the rightmost cells remain polarized. Because of their low conductance ratio $G^{\circ}_{pol}/G^{\circ}_{dep} = 0.2$, the leftmost depolarized cells can resist the polarizing effect from the rightmost polarized cells (Fig. 3(a)) and thus a two-region polarization pattern is established for the case of weak chain connectivity.

On the contrary, when the intercellular coupling is sufficiently high, a *polarity transition* occurs at a critical ratio of λ/d from which the leftmost cells can no longer resist the dominant polarization enforced by the rightmost cells (Fig. 3(a); see also Fig. 2 for the role of $G^{\circ}_{pol}/G^{\circ}_{dep}$). Thus, the chain state depends on both the individual cell characteristics (Fig. 2) and the intercellular cou-

pling (Fig. 3(a)). Note also that this bioelectrical state modulates the spatio-temporal distribution of signaling ions and molecules across the system. However, these distributions can evolve over experimental times much longer than those obtained here because of the high number of cells and the slow diffusion-reaction processes typical of real systems [2,3,11].

Figs. 3(b) and (c) show the effects of cutting a central fragment whose size increases from left to right in the cases of low and high intercellular coupling; see Fig. 3(a). The fragment of the multicellular system is located around the cell #60. The system is assumed to be at steady-state conditions before the cut (Fig. 3(a)). Immediately after the cut, the leftmost and rightmost cells have the potentials corresponding to their initial positions in the system. After a sufficiently long time, however, the central fragment reaches a new steady-state whose polarity depends on the region intercellular coupling and size (number of cells). Note in particular the polar ($\lambda/d = 1$) and non-polar ($\lambda/d = 4$) characteristics of the electric potential obtained in each case. This fact, together with the minimum number of cells required to avoid an isopotential fragment and establish polarity, provide qualitative explanations to the bioelectrical morphologies experimentally observed in planaria [2,11,18].

While Fig. 3 is illustrative of multicellular bioelectrical patterns, it is restricted to a particular case study. To better understand the influence of the single-cell conductance G°_{pol} and the intercellular conductance G° on the chain bioelectrical polarity, Fig. 4 presents a configurational *phase space* in terms of the bioelectrical characteristics that regulate the chain polarity: the relative channel conductance difference $\Delta G^{\circ}_{\text{pol}}/G_{\text{ref}}$ between the chain ends that establishes the chain asymmetry prepattern, the relative coupling conductance G°/G_{ref} characteristic of the intercellular connectivity, and the number N of cells in the chain which gives the chain length L. The conductances are scaled to the common reference conductance $G_{\text{ref}} = G^{\circ}_{\text{dep}}$. Note that the tridimensional (3D) phase space of Fig. 4 has significant differences with respect to previous 2D spaces [18]: it assumes constant gap junction conductances but includes voltage-gated ion channels and, more importantly, it shows the effect of the number of cells in the system.

As expected, the decrease of the bioelectrical gradient slope $\Delta G^{\circ}_{\text{pol}}/G_{\text{ref}}$ inhibits the system polarity and results in quasi-symmetrical patterns where the electric potential pattern cannot encode a depolarized (*head*)-polarized (*tail*) morphology (curves #2 and #3 of Fig. 4). Experimentally, the slopes of electrochemical gradients are crucial for proper development of epithelial polarity [1]. Also, the increase of the gap junction conductance G°/G_{ref} decreases the polarity (curves #1 and #3 of Fig. 4) because the intercellular connectivity enforces isopotential patterns via the intercellular currents I_{ij} of Fig. 1 [2,11,12,28]. For $G^{\circ}/G_{\text{ref}} > 1$, Fig. 3 shows that the two region pattern required to establish polarity in Fig. 4 begins to be smoothed. On the contrary, decreasing G°/G_{ref} can facilitate polarity. In qualitative agreement with this result, after octanol blocking of intercellular gap junctions, the number of isopotential regions in planaria pseudo morphologies is increased because of decreased connectivity [28]. Interestingly, the model predicts also that a minimum number N of cells is needed for the chain polarity to be established (curves #1 and #2 of Fig. 4). Although this prediction has also been observed in experimental model systems, the fact is that not only the electrical polarity but also the morphogen distribution, together with the number and type of cells involved in regeneration, are important [2,8–11]. The critical system size allowing a polar morphology decreases with $\Delta G^{\circ}_{\text{pol}}/G_{\text{ref}}$ (curve #2 of Fig. 4) and increases with G°/G_{ref} (curve #1 of Fig. 4), as it could be expected. The model of Fig. 1 and equation (1) could now be extended to include a heterogeneous distribution of gap junctions, a case of experimental interest

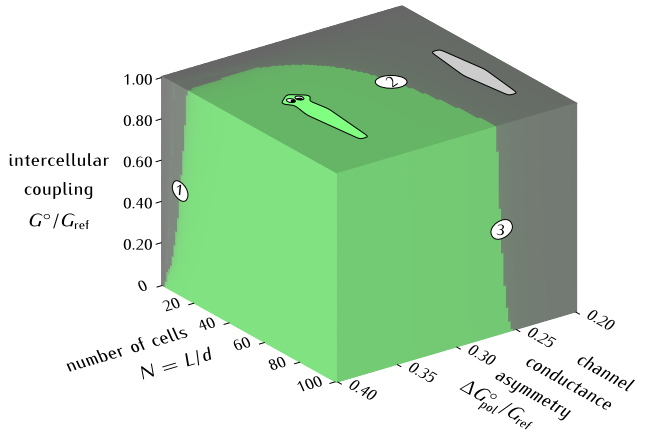

Fig. 4. The configurational phase space shows the polar (*green*) and non-polar (*grey*) chain states as a function of the bioelectrical characteristics: the channel conductance asymmetry $\Delta G^{\circ}_{\text{pol}}/G_{\text{ref}}$ between the chain ends ($G^{\circ}_{\text{pol}}/G_{\text{ref}} = 0.2$ for cell #1 and $G^{\circ}_{\text{pol}}/G_{\text{ref}} = 0.5$ for cell $\#N = 100$), the intercellular coupling provided by the gap junction conductance G°/G_{ref}, and the system size described by the number N of cells in the chain of length $L = Nd$. The numbers in the curves correspond to processes at constant $\Delta G^{\circ}_{\text{pol}}/G_{\text{ref}}$ (curve #1), constant G°/G_{ref} (curve #2), and constant N (curve #3). The insets show schematically the different polarity states obtained from equation (1).

[22,28,30]. In particular, the model could allow a prepattern of G°/G_{ref} rather than of $G^{\circ}_{\text{pol}}/G^{\circ}_{\text{dep}}$ values throughout the chain as well as voltage-gated gap junctions, which influences polarity [18].

Fig. 4 can also be interpreted as a *configurational memory space* which is in qualitative agreement with experiments conducted in planarian systems [2,11,18,28]. In particular, the weakening of the gap junction conductance induced by blocking agents such as octanol [28] can be modeled in our case by decreasing the intercellular conductance G°/G_{ref} and gives and increase in the number of approximately isopotential regions from one to two (see curves #1 and #3 here). Also, external actions on polarizing agents such as H,K-ATPase inhibitors and depolarizing agents such as the nigericin ion pump modify both the electric potential gradient through the model animal and the observed polarity [2,11,18]. These actions can be mimicked in the model by changes in the conductance difference $\Delta G^{\circ}_{\text{pol}}/G_{\text{ref}}$ between the chain ends (curves #2 and #3). Experimentally, particular spatio-temporal distributions of channel and gap junction conductances can be established by local mRNA microinjections, optogenetic stimulation, and external blockers [2,3,14,16,28,29].

In addition to the long range polarity caused by a gradual change of the *pol* channel protein throughout the chain (Fig. 3), small polar domains periodically distributed can also be relevant in multicellular development (Fig. 5). In early embryonic patterning, specific cells which have acquired individual characteristics over local regions can trigger development into tissues and organs. This is the case of self-assembled cells with different genetic identity exhibiting inhibition and sorting patterns [31]. Fig. 5 considers the case of a spatially periodic arrangement of depolarized/polarized domains composed of cells which have $G^{\circ}_{\text{pol}}/G^{\circ}_{\text{dep}} = 0.2$ and $G^{\circ}_{\text{pol}}/G^{\circ}_{\text{dep}} = 0.5$ alternately.

Because the polarized state is the dominant stable solution (Fig. 3), the stationary patterns of Fig. 5 can deviate from this state only when the number of cells in the domain is sufficiently high to establish a *local community polarization*; compare the heterogeneous patterns of the domains having 10 and 20 cells with the quasi-homogeneous pattern obtained for the 5-cells domain. Note also that the multicellular coupling length λ should be sufficiently small to preclude the long range correlations of Fig. 3. Indeed, when the intercellular coupling is strong, the dominant polarization state is enforced through the chain, as suggested by Fig. 3 in

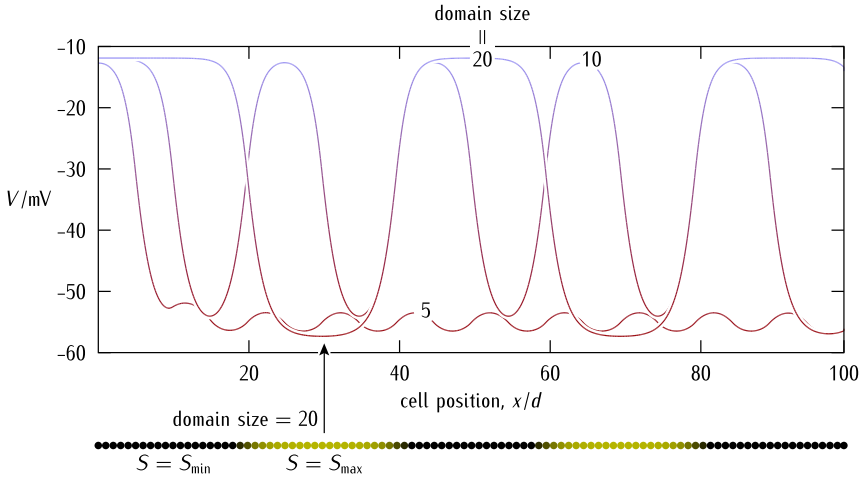

Fig. 5. A multicellular chain composed of periodic domains shows short order polarization patterns when the intercellular coupling conductance is low and the number of cells in the domain is sufficiently high. The steady-state potential patterns are obtained from equation (1) and corresponds to the coupling conductance $G^\circ/G_{\text{ref}} = 1.0$ and $t = 5\,000$ s. The cells are grouped in domains of 5, 10, and 20 cells that are distributed in alternate regions of $G^\circ_{\text{pol}}/G^\circ_{\text{dep}} = 0.2$ and $G^\circ_{\text{pol}}/G^\circ_{\text{dep}} = 0.5$. The *bottom illustration* shows schematically the concentration profile of a positively charged signaling ion or molecule S whose minimum and maximum values are locally regulated by the electric potential pattern established over domains of 20 cells (*bottom*).

the high $G^\circ/G^\circ_{\text{dep}}$ limit. In general, morphological outcomes result from the local interplay between signaling agents and electric potentials [3,4,14], as shown schematically for the case of a domain with 20 cells in Fig. 5 (*bottom*).

4. Conclusion

Fig. 1 and equation (1) constitute a minimal toy model for multicellular bioelectric states, as shown by the configurational space of Fig. 4. In particular, Fig. 1 shows that the bi-stability of the polarized and depolarized single-cell states (Fig. 2) together with the intercellular connectivity (Figs. 1 and 3) can allow long and short order polar patterns (Figs. 3–5) that depend on the system size. Because of the coupling between bioelectrical and biochemical signals, these patterns eventually emerge as morphological outcomes [1,2,11,18,28]. This result can also be relevant to synthetic morphology [32,33] because the supervised establishment of polarity can be assisted by acting on bioelectrical patterns [27].

Declaration of competing interest

The authors declare that they have no known competing financial interests or personal relationships that could have appeared to influence the work reported in this paper.

Acknowledgements

J.C., J.A.M. and S.M. acknowledge the financial support of the *Ministerio de Ciencia e Innovación* (Spain) and the European Regional Development Funds (FEDER) jointly cofinancing grant No. PGC2018-097359-B-I00.

References

[1] S.K. Schotthöfer, J. Bohrmann, Bioelectrical and cytoskeletal patternscorrelate with altered axial polarity in thefollicular epithelium of the drosophila mutant gurken, BMC Dev. Biol. 20 (2020) 5, https://doi.org/10.1186/s12861-020-00210-8.

[2] F. Durant, J. Bischof, C. Fields, J. Morokuma, J. LaPalme, A. Hoi, M. Levin, The role of early bioelectric signals in the regeneration of planarian anterior/posterior polarity, Biophys. J. 116 (2019) 948–961, https://doi.org/10.1016/j.bpj.2019.01.029.

[3] K.A. McLaughlin, M. Levin, Bioelectric signaling in regeneration: mechanisms of ionic controls of growth and form, Dev. Biol. 433 (2018) 177–189, https://doi.org/10.1016/j.ydbio.2017.08.032.

[4] J. Cervera, A. Pietak, M. Levin, S. Mafe, Bioelectrical coupling in multicellular domains regulated by gap junctions: a conceptual approach, Bioelectrochemistry 123 (2018) 45–61, https://doi.org/10.1016/j.bioelechem.2018.04.013.

[5] M.Z. Brodsky, M. Levin, From physics to pattern: uncovering pattern formation in tissue electrophysiology, Artif. Life Conf. Proc. 30 (2018) 351–358, https://doi.org/10.1162/isal_a_00066.

[6] L.A. Kadir, M. Stacey, R. Barrett-Jolley, Emerging roles of the membrane potential: action beyond the action potential, Front. Physiol. 9 (2018) 1661, https://doi.org/10.3389/fphys.2018.01661.

[7] H. Meinhardt, Turing's theory of morphogenesis of 1952 and the subsequent discovery of the crucial role of local self-enhancement and long-range inhibition, Interface Focus 2 (2012) 407–416, https://doi.org/10.1098/rsfs.2011.0097.

[8] T. Stückemann, J.P. Cleland, S. Werner, H.T.-K. Vu, R. Bayersdorf, S.-Y. Liu, B. Friedrich, Frank Jülicher, J.C. Rink, Antagonistic self-organizing patterning systems control maintenance and regeneration of the anteroposterior axis in planarians, Dev. Cell 40 (2017) 248–263, https://doi.org/10.1016/j.devcel.2016.12.024.

[9] P.W. Reddien, The cellular and molecular basis for planarian regeneration, Cell 175 (2018) 327–345, https://doi.org/10.1016/j.cell.2018.09.021.

[10] A.G. Tewari, S.R. Stern, I.M. Oderberg, P.W. Reddien, Cellular and molecular responses unique to major injury are dispensable for planarian regeneration, Cell Rep. 25 (2018) 2577–2590, https://doi.org/10.1016/j.celrep.2018.11.004.

[11] F. Durant, J. Morokuma, C. Fields, K. Williams, D.S. Adams, M. Levin, Long-term, stochastic editing of regenerative anatomy via targeting endogenous bioelectric gradients, Biophys. J. 112 (2017) 2231–2243, https://doi.org/10.1016/j.bpj.2017.04.011.

[12] A. Pietak, M. Levin, Bioelectrical control of positional information in development and regeneration: a review of conceptual and computational advances, Prog. Biophys. Mol. Biol. 137 (2018) 52–68, https://doi.org/10.1016/j.pbiomolbio.2018.03.008.

[13] I. Weiß, J. Bohrmann, Electrochemical patterns during Drosophila oogenesis: ion-transport mechanisms generate stage-specific gradients of ph and membrane potential in the follicle-cell epithelium, BMC Dev. Biol. 19 (2019) 12, https://doi.org/10.1186/s12861-019-0192-x.

[14] J. Cervera, M. Levin, S. Mafe, Bioelectrical coupling of single-cell states in multicellular systems, J. Phys. Chem. Lett. 11 (2020) 3234–3241, https://doi.org/10.1021/acs.jpclett.0c00641.

[15] M. Léonetti, E. Dubois-Violette, F. Homblé, Pattern formation of stationary transcellular ionic currents in fucus, Proc. Natl. Acad. Sci. USA 101 (2004) 10243–10248, https://doi.org/10.1073/pnas.0402335101.

[16] H.M. McNamara, R. Salegame, Z.A. Tanoury, H. Xu, S. Begum, G. Ortiz, O. Pourquie, A.E. Cohen, Bioelectrical domain walls in homogeneous tissues, Nat. Phys. 16 (2020) 357–364, https://doi.org/10.1038/s41567-019-0765-4.

[17] R.D. Kirkton, N. Bursac, Engineering biosynthetic excitable tissues from unexcitable cells for electrophysiological and cell therapy studies, Nat. Commun. 2 (2011) 300, https://doi.org/10.1038/ncomms1302.

[18] J. Cervera, S. Meseguer, M. Levin, S. Mafe, Bioelectrical model of head-tail patterning based on cell ion channels and intercellular gap junctions, Bioelectrochemistry 132 (2020) 107410, https://doi.org/10.1016/j.bioelechem.2019.107410.

[19] B. Hille, Ion Channels of Excitable Membranes, 3rd edition, Sinauer Associates, 1992.

[20] J. Cervera, S. Meseguer, S. Mafe, The interplay between genetic and bioelectrical signaling permits a spatial regionalisation of membrane potentials in model multicellular ensembles, Sci. Rep. 6 (2016), https://doi.org/10.1038/srep35201.
[21] S.Y. Shvartsman, R.E. Baker, Mathematical models of morphogen gradients and their effect on gene expression, WIREs Dev. Biol. 1 (2012) 715–730, https://doi.org/10.1002/wdev.55.
[22] J. Cervera, V. Pai, M. Levin, S. Mafe, From non-excitable single-cell to multicellular bioelectrical states supported by ion channels and gap junction proteins: electrical potentials as distributed controllers, in: Progress in Biophysics and Molecular Biology, 2019.
[23] V. Zhdanov, Kinetic models of gene expression including non-coding rnas, Phys. Rep. 500 (2011) 1–42, https://doi.org/10.1016/j.physrep.2010.12.002.
[24] V.P. Zhdanov, A neuron model including gene expression: bistability, long-term memory, etc., Neural Process. Lett. 39 (2014) 285–296, https://doi.org/10.1007/s11063-013-9304-y.
[25] O.V. Aslanidi, O.A. Mornev, O. Skyggebjerg, P. Arkhammar, O. Thastrup, M.P. Sørensen, P.L. Christiansen, K. Conradsen, A.C. Scott, Excitation wave propagation as a possible mechanism for signal transmission in pancreatic islets of Langerhans, Biophys. J. 80 (2001) 1195–1209, https://doi.org/10.1016/S0006-3495(01)76096-1.
[26] S.M. Busse, P.T. McMillen, M. Levin, Cross-limb communication during xenopus hindlimb regenerative response: non-local bioelectric injury signals, Development 145 (2018) dev164210, https://doi.org/10.1242/dev.164210.
[27] J. Mathews, M. Levin, The body electric 2.0: recent advances in developmental bioelectricity for regenerative and synthetic bioengineering, Curr. Opin. Biotechnol. 52 (2018) 134–144, https://doi.org/10.1016/j.copbio.2018.03.008.
[28] M. Emmons-Bell, F. Durant, J. Hammelman, N. Bessonov, V. Volpert, J. Morokuma, K. Pinet, D.S. Adams, A. Pietak, D. Lobo, M. Levin, Gap junctional blockade stochastically induces different species-specific head anatomies in genetically wild-type girardia dorotocephala flatworms, Int. J. Mol. Sci. 16 (2015) 27865–27896, https://doi.org/10.3390/ijms161126065.
[29] V. Pai, A. Pietak, V. Willocq, B. Ye, N.-Q. Shi, M. Levin, HCN2 rescues brain defects by enforcing endogenous voltage pre-patterns, Nat. Commun. 9 (2018) 998, https://doi.org/10.1038/s41467-018-03334-5.
[30] C.M. Glen, T.C. McDevitt, M.L. Kemp, Dynamic intercellular transport modulates the spatial patterning of differentiation during earlyneural commitment, Nat. Commun. 9 (2018) 4111, https://doi.org/10.1038/s41467-018-06693-1.
[31] D.A. Turner, P. Baillie-Johnson, A. Martinez-Arias, Organoids and the genetically encoded self-assembly of embryonic stem cells, BioEssays 38 (2016) 181–191, https://doi.org/10.1002/bies.201500111.
[32] N. Luo, S. Wang, L. You, Synthetic pattern formation, Biochemistry 58 (2019) 1478–1483, https://doi.org/10.1021/acs.biochem.8b01242.
[33] J.J. Velazquez, E. Su, P. Cahan, M.R. Ebrahimkhani, Programming morphogenesis through systems and synthetic biology, Trends Biotechnol. 36 (2018) 415–429, https://doi.org/10.1016/j.tibtech.2017.11.003.